Precipitation of Hydroxyapatite at 37 °C in a Meso Oscillatory Flow Reactor Operated in Batch at Constant Power Density

Filipa Castro
Institute for Biotechnology and Bioengineering (IBB), Centre for Biological Engineering, Dept. of Biological Engineering, University of Minho, Campus de Gualtar, Braga 4710-057, Portugal

António Ferreira
Institute for Biotechnology and Bioengineering (IBB), Centre for Biological Engineering, University of Minho, Campus de Gualtar, Braga 4710-057, Portugal

LEPAE-Laboratory for Process, Environmental and Energy Engineering, Dept. of Chemical Engineering, Faculty of Engineering of the University of Porto, Rua Roberto Frias, s/n, Porto 4200-465, Portugal

Fernando Rocha
LEPAE-Laboratory for Process, Environmental and Energy Engineering, Faculty of Engineering of the University of Porto, Rua Roberto Frias, s/n, Porto 4200-465, Portugal

António Vicente and José António Teixeira
Institute for Biotechnology and Bioengineering (IBB), Centre for Biological Engineering, University of Minho, Campus de Gualtar, Braga 4710-057, Portugal

DOI 10.1002/aic.14193
Published online July 29, 2013 in Wiley Online Library (wileyonlinelibrary.com)

A meso oscillatory flow reactor (meso-OFR) was successfully applied for the precipitation of hydroxyapatite (HAp) nanoparticles. Mixing efficiency of the mesoreactor operated batchwise in a vertical tube was evaluated at constant power density, by monitoring variation of hue values upon mixing both spatially and temporally. The best operating conditions for fast mixing and a more homogeneous reaction medium were verified for $f = 0.83$ Hz and $x_0 = 4.5$ mm. HAp precipitation was then carried out under these conditions at 37 °C for different mixing Ca/P molar ratios. HAp nanoparticles with a mean size (d_{50}) of about 67 nm and a narrow size distribution were obtained. Furthermore, the obtained results show the advantages of the meso-OFR over a stirred tank batch reactor due to the production, about four times faster, of smaller and more uniform HAp nanoparticles. © 2013 American Institute of Chemical Engineers *AIChE J*, 59: 4483–4493, 2013
Keywords: precipitation, hydroxyapatite, mixing, mesoreactor, oscillatory flow

Introduction

Hydroxyapatite (HAp), $Ca_5(PO_4)_3OH$, has been extensively used in bone replacement applications due to its biocompatibility, bioactivity, and osteoconductivity.[1] In this context, it is desirable that HAp crystals meet specific requirements such as high specific surface area (favored by small crystal size), narrow size distribution, and high purity, in order to optimize bone-related cells growth around them.[2,3]

HAp is usually prepared by precipitation from solution in stirred tank batch reactors.[4] In this type of system, inhomogeneous distribution of the mixing power and energy within the process volume leads to a heterogeneous distribution of supersaturation in the reaction medium, thus affecting crystal size distribution and chemical purity of the particles precipitated. The problem becomes magnified as the scale of operation increases and can be particularly pronounced in fast precipitation systems.[5] This calls for the development of a system that provides an efficient and intense mixing.

In recent years, oscillatory flow reactors (OFRs) have been extensively studied in chemical engineering processes, namely in crystallization.[6,7] OFRs have been proved to result into significant enhancement in processes such as mass transfer,[8] particle mixing, and separation.[9] The basic concept of an OFR is the application of periodic fluid oscillations to a cylindrical column containing evenly spaced orifice baffles.[10] The OFR can be operated batchwise or continuously in horizontal or vertical tubes. The liquid or multiphase fluid is typically oscillated in the axial direction by means of diaphragms, bellows, or pistons, at one or both ends of the tube, developing an efficient mixing mechanism (oscillatory flow mixing), where mixing intensity is controlled by the oscillation frequency and amplitude. The flow direction is periodically reversing and this motion interacts with the constrictions forming vortices. This provides precise control of mixing, from gentle to the most intense, and efficient heat and mass transfer.[11–13] The "conventional" OFR geometry

Correspondence concerning this article should be addressed to F. Castro at fcastro@deb.uminho.pt.

was redesigned to suit some of the bioprocess applications requirements.[10,13,14] The reactor is a mesoscale (milliliter) device with smooth periodic constrictions, thus reducing reagent requirements and waste.[10] It can also be easily scaled up to the industrial level.[15] In that way, the meso-OFR appears as a good candidate to promote ideal conditions for the controllability of HAp particles properties.

Imaging-based and colorimetric techniques for crystallization monitoring have been investigated, in particular, for the evaluation of growth kinetics[16–19] and mixing.[20] The present work focuses on mixing and pH monitoring, as both are key parameters when studying calcium phosphates precipitation. On one hand, mixing effects are significant in determining the distribution of supersaturation and subsequently in determining the product properties (purity, morphology, size, and size distribution),[21] as fast or very fast chemical reactions are often involved in precipitation systems. Conversely, pH is an important parameter in determining the likelihood of the formation of calcium phosphate phases.[22] The influence of pH in the formation of calcium phosphates is linked to the properties of phosphate containing solutions. Due to the triprotic equilibrium in these systems, variations in pH alter the relative concentrations of the four protonated forms of phosphoric acid and thus both the chemical composition and the amount of the CaP formed by direct precipitation.[23] As to the evaluation of the mixing performance, global measurement optically based methods offer many advantages over local measurement probes, namely the capability to identify the unmixed zones and to measure the end point of the intimate mixing in the whole reactor.[24] Further, they are nonintrusive and they do not perturb the flow.[24] In the present work, mixing was monitored by "color" measurements.[25] The technique uses the hue instead of the intensity (or brightness), enabling the use of multiple colors in a manner not possible with traditional methods that use grayscale or a specific color channel, for example, the red component of the RGB color space.[24] Concerning pH monitoring, conventional glass-type electrodes have been widely used. However, they possess several constraints when implemented in scaled-down reactors due to their size, rigidity, inflexibility,[26] and response time. The methodology used in this work for pH monitoring attempts to address part of these limitations. pH was estimated on the basis of the changes in solution absorbance. The absorbance spectra were recorded with an optical fiber.

This article reports on the feasibility of a meso-OFR to improve the precipitation process of HAp under near-physiological conditions of temperature and pH, particularly important when preparing HAp for medical purposes. Indeed, it is important to follow specific criteria for pH and temperature in order to promote more conductive conditions for the survival of bone-related cells.[1] First, mixing efficiency of the mesoreactor operated in batch in a vertical tube at a constant powder density (31.5 $W \cdot m^{-3}$) was evaluated by monitoring the hue. HAp precipitation process was then studied for different mixing Ca/P molar ratios (1.00, 1.33, and 1.67), where pH was continuously monitored. Experiments were performed under the same conditions of temperature (37 °C), reactants concentration, and power density applied in a stirred tank batch reactor.[27] The constant power density applied to both reactors was used as the reference criterion. The effectiveness of both mixing methods for a given power input was evaluated in terms of reaction time and characteristics of the precipitated particles.

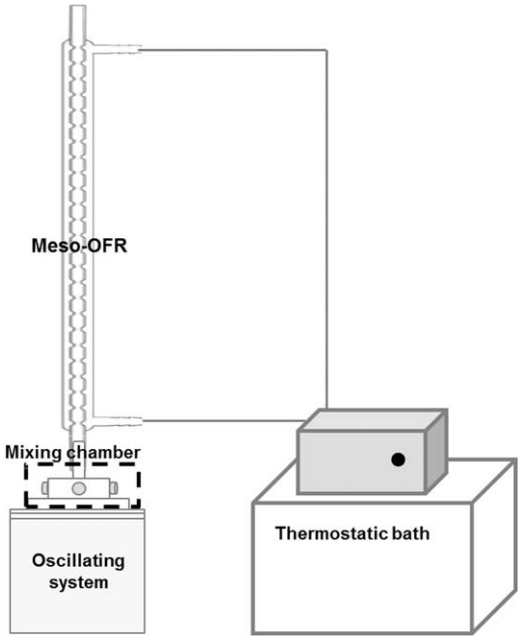

Figure 1. Experimental set-up for evaluation of mixing and precipitation of HAp.

Materials and Methods

Description of the experimental set-ups

Meso-OFR. The mesoreactor consists of a 35 cm long and 4.4 mm internal diameter glass jacketed tube provided with smooth periodic cavities, with an averaged baffle spacing of 13 mm and a baffle thickness of 6 mm.[10] The diameter on the constricted zone (baffle internal diameter) is 1.6 mm, leading to a baffle free area of 13%.[10] The reactor has an approximate volume of 4 mL.

The fluid was oscillated using a piston moved by a stirring motor (R100C, CAT). The oscillating system was purposely designed. Oscillation amplitudes and frequencies were ranging from 1 to 4.5 mm and 0.83 to 3.67 Hz (50 to 220 rpm), respectively. Values of the amplitudes correspond to the center-to-peak amplitude and these measurements were performed in the tube without constrictions.

Experimental Apparatus for Evaluation of Mixing and HAp Precipitation. The experimental set-up used for studying the mixing efficiency of the meso-OFR and HAp precipitation is presented in Figure 1.

The reactants were fed into the set-up one at a time by means of a syringe pump (NE-4000), using syringes of 5 mL (BD Plastipak). Temperature inside the meso-OFR was regulated by a thermostatic bath maintained at 37°C.

Experimental Apparatus for pH Monitoring. As pH is a crucial parameter in HAp precipitation and given the small dimensions of the reactor, monitoring of pH was done with an optical fiber. It allowed monitoring pH variation over time during HAp precipitation process. It must be pointed out that the resulting HAp crystals cannot be used for characterization due to the use of a chemical pH indicator in this process. So, this apparatus was only used to obtain the pH profile during HAp precipitation.

In order to validate this methodology, the pH of the final suspensions was measured using a pH microelectrode (SenTix Mic-D, WTW) and compared with the final values obtained using an optical fiber system. The experimental set-up used for pH monitoring is presented below (Figure 2).

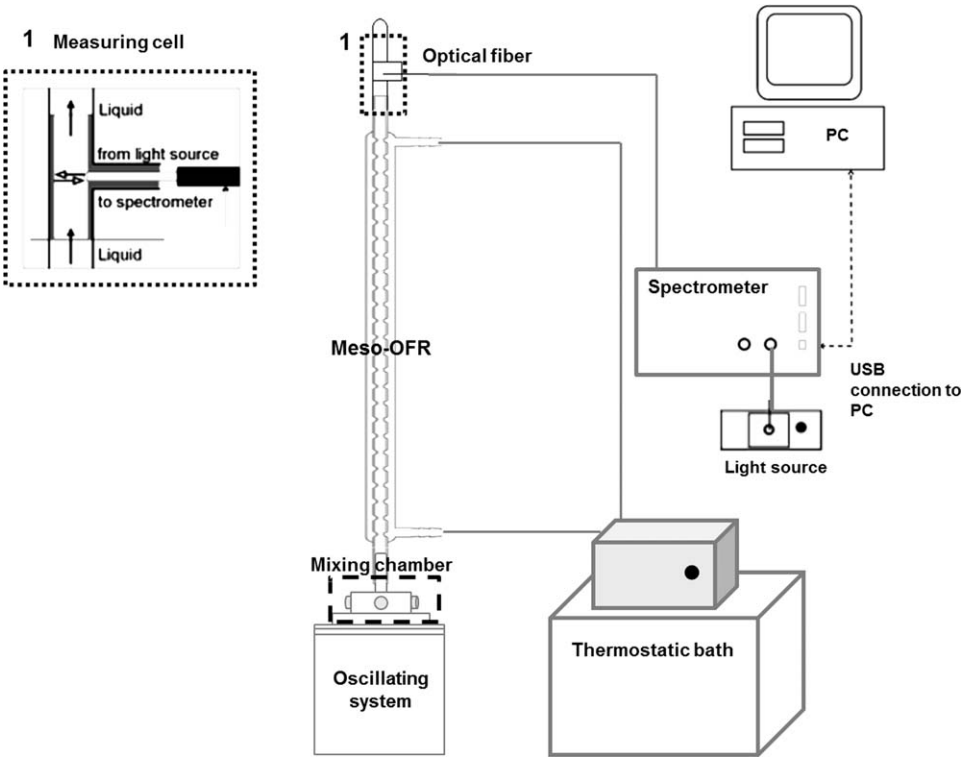

Figure 2. Experimental set-up for pH monitoring.

In-line pH value was obtained from the absorbance measured via an optical microprobe (reflection probe, tip 1.5 mm, FCR–7UV200–1.5x100-2, Avantes, Eerbeek, The Netherlands) connected to a multichannel optic spectrometer system (Avantes, Eerbeek, The Netherlands). The probe was installed at the outlet of the meso-OFR, perpendicularly to the flow direction into a 4-mm internal diameter in-line flow cell with white walls (Swagelok) covered by black adhesive tape (Figure 2). Readings were taken every 2 s.

The meso-OFR was completely covered by an aluminum foil to reduce the noise due to ambient light.

Mixing efficiency of the meso-OFR operated in batch mode for a power density of 31.5 W·m^{-3}

Mixing efficiency of the meso-OFR operated in batch was evaluated under the same conditions of power density (31.5 W m^{-3}) applied in a stirred tank batch reactor.[27]

The power density of the stirred tank batch reactor was estimated through the following equation[28]

$$\frac{P}{V} = \frac{N_P \rho N^3 D_s^5}{\pi D_t^2 \left(\frac{L}{4}\right)} \quad (1)$$

where P/V is the power density (W m^{-3}), ρ is the fluid density (kg m^{-3}), N is the speed of the stirrer (s^{-1}), D_s is the diameter of the stirrer (m), D_t is the diameter of the tank (m), and L is the height of the tank (m) and N_P is the dimensionless power number of the stirrer.

The final power density was determined multiplying the power density by the number of agitators that, according to the configuration of the stirrer used is 16.[27]

Regarding the power density of the meso-OFR, it was estimated from[12]

$$\frac{P}{V} = \frac{2\rho N_B}{3\pi C_D^2} \frac{1-\alpha^2}{\alpha^2} x_0^3 \omega^3 \quad (2)$$

where N_B is the number of constrictions per unit length (m^{-1}), α the baffle free area ratio [$=(D_0/D)^2$] where D_0 is the constriction diameter (m) and D is the tube diameter (m), x_0 the oscillation amplitude (m), ω the angular frequency of oscillation ($=2\pi f$), and C_D the baffle discharge coefficient.

The parameters needed to determine the power density of both reactors are presented in Table 1. The fluid density of water was used as the solutions used are low concentrated aqueous solutions. As to the power number of the stirrer (N_P), it was estimated based on the stirrer design and on the relationship between the power number (N_P) and the Reynolds number (Re) for Newtonian liquids.[29] Concerning the parameters of the meso-OFR, values are based in Reis work.[10]

Table 1. Parameters for the Estimation of the Power Density of the Stirred Tank Batch Reactor and the Meso-OFR

	N_P	ρ (kg m^{-3})	N (s^{-1})	D_s (m)	D_t (m)	L (m)
Stirred tank batch reactor	1.25	993.329	4.5	0.029	0.1	0.15
	N_B (m^{-1})	ρ (kg m^{-3})	α	C_D	x_0 (m)	ω (rad s^{-1})
Meso-OFR	76.92	993.329	0.13	0.6	–	–

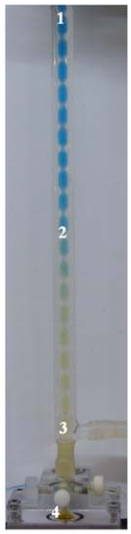

Location Number	1	2	3	4
Part of the meso-OFR	Top	Middle	Bottom	Cone

Figure 3. Picture of the meso-OFR.

The numeric label indicates the locations at which the quantification of the hue was carried out. [Color figure can be viewed in the online issue, which is available at wileyonlinelibrary.com.]

Through Eq. 2, it is possible to obtain a relation between the oscillation amplitude (x_0) and the frequency of oscillation (f) for a given power input. One of the parameters (x_0 or f) was fixed in order to determine the other one. According to this, three different mixing conditions were defined: $f = 3.67$ Hz and $x_0 = 1$ mm; $f = 1.67$ Hz and $x_0 = 2.25$ mm; $f = 0.83$ Hz and $x_0 = 4.5$ mm.

Mixing performance was evaluated using a colorimetric technique by measuring the hue, enabling thus the use of multiple colors. This method has been developed by Rezk et al.[25] to evaluate the mixing performance of paper-based microfluidic systems. They proposed hue instead of intensity (or brightness) as an independent means to quantify mixing. In fact, each color is characterized by a base hue value, independently of intensity, and hence independently of the method and consistency of the illumination.[25] Although traditional colorimetric methods are based on grayscale or a specific color channel, for example, the red component of the RGB color space,[25] this technique enables the use of multiple colors. In addition, the method provides the ability to dynamically track the progression of the color change both in space and time without requiring a large color contrast as required when using grayscale analysis. Moreover, the hue values vary linearly with the color scale, making it a robust method under different lighting conditions.

A camera (SONY Cyber-shot DSC-H10) was used to photograph the fluid inside the meso-OFR at different time intervals. Hue of the fluid was determined at four specific locations (Figure 3) by specific software (NIS-Elements) for the different mixing (f and x_0 values) conditions defined.

Two buffer solutions, $(NH_4)H_2PO_4$ ($0.2\ mol \cdot L^{-1}$) (Merck) and NH_3 ($0.1\ mol \cdot L^{-1}$) (Pronolab), were prepared. A pH indicator, bromothymol blue $1g \cdot L^{-1}$ (Panreac), was added to both solutions (2 mL per 100 mL of solution), resulting with two solutions of different colors, one yellow corresponding to the acidic solution, and one blue corresponding to the basic solution. The average hue of each buffer solution, as well as of the resulting solution of the mixture in equal amounts of the two buffer solutions, were estimated. For that, the solutions were fed into the meso-OFR (Figure 1) and their corresponding hue was estimated based on the average of the hue values measured at different locations (Figure 3). The yellow solution has a hue of approximately 33.52 and the blue solution has a hue around 142.06. The solution resulting from the mixture in equal amounts of the two buffer solutions has a hue of approximately 70.95, corresponding to a green solution and will be referred as "Green Hue" in the rest of the text. Mixing efficiency of the meso-OFR operated in batch was then evaluated by the mixing of equal amounts (2.8 mL) of the buffer solutions under different mixing conditions (f and x_o values defined previously). The basic solution was first injected slowly, to avoid the formation of bubbles inside the mesoreactor, and then the acidic solution injected rapidly (3 to 4 s), in order to simulate the HAp precipitation process studied.

Monitoring of pH

Monitoring of pH was performed in the experimental apparatus presented in Figure 2. The optical response of the microprobe was calibrated by running several solutions with different pH values. For that, 0.5 L of equimolar (0.01926 mol L^{-1}) calcium hydroxide (Riedel-de Haën, 96%) and orthophosphoric acid (Pronalab, 85%) aqueous solutions were prepared, 1 mL of bromothymol blue ($1g\ L^{-1}$) (Panreac) being added to each solution. Then, several solutions with different pH were prepared by mixing the dyed calcium hydroxide and orthophosphoric acid aqueous solutions in different proportions. Afterward, the resulting solutions were injected in the meso-OFR for the measurement of the absorbance.

The addition of bromothymol blue allows monitoring the changes of pH through the measurement of the absorbance. Bromothymol blue has two peaks of absorption, one at 430–435 nm for acidic solutions and one at 615–618 nm for basic solutions. In this study, the pH varies between approximately 6 and 12, therefore, it was only used the information relative to the blue absorption peak (615–618 nm).

Three parameters were measured simultaneously:

- Spectrum in the visible $\lambda = 400$–700 nm;
- $F_1 = \int_{610nm}^{620nm} A(\lambda)d\lambda$, which corresponds to the blue absorption peak;
- $F_2 = \int_{690nm}^{700nm} A(\lambda)d\lambda$, which corresponds to a "neutral" zone;

where λ is the wavelength and $A(\lambda)$ is the light absorbance.

F_2 was measured in order to monitor the noise. F_1-F_2 (Abs) corresponds to the parameter used for the construction of the calibration curve. The experiments were carried out at 37 °C and repeated three times. The reference blank used was ultrapure water. Experiments showed that the relation between absorbance (Abs) and pH is linear only for pH between 6.3 and 8.

pH of the final suspension was also measured by a pH microelectrode (SenTix Mic-D, WTW) in order to compare with the final values obtained from the absorbance measurement.

It is important to mention that this methodology was used exclusively for pH monitoring. Due to the use of the pH indicator, bromothymol blue, crystals obtained cannot be

Table 2. Operating Conditions for the Precipitation of HAp and Characteristics of the Final Product

$[CaOH_2]$ (mol L^{-1})	$[H_3PO_4]$ (mol L^{-1})	Mixing Ca/P Molar Ratio	Final pH Measured by the pH Microelectrode	Final pH Obtained from the Absorbance Measurements	Final Ca/P Molar Ratio
0.01926	0.01926	1.00	5.9	6.3	1.36 ± 0.02
	0.01448	1.33	6.4	6.5	2.10 ± 0.02
	0.01154	1.67	7.2	7.3	1.46 ± 0.03

used for characterization. Indeed, bromothymol blue can affect the composition of the resulting precipitated HAp particles.

Precipitation of HAp

Powder Preparation. HAp was synthesized by the mixing of a saturated calcium hydroxide (Riedel-de Haën, 96%) aqueous solution and an orthophosphoric acid (Pronalab, 85%) aqueous solution. 0.5 L of both reactants were prepared with ultrapure water (Milli Q water, resistivity of 18.2 $M\Omega \cdot cm^{-1}$ at 25 °C) and their ionic force adjusted by the addition of 6 mL of potassium chloride (Mallinckrodt, 99.8%) 4 $mol \cdot L^{-1}$ solution. To facilitate the dissolution of calcium hydroxide, the solution was agitated in a closed vessel for 24 h at 500 rpm and at 25°C, as its solubility decreases with temperature increase.[30] Then, both reactants were heated and kept at 37 °C.

The precipitation process was carried out under the same conditions of temperature (37 °C), reactants concentration, and power density (31.5 $W \cdot m^{-3}$) used in a stirred tank batch reactor.[27] Further, HAp precipitation was studied for three different mixing Ca/P molar ratios, 1.00, 1.33, and 1.67 (Table 2). Equal volumes (2.8 mL) of reactant solutions were injected. The calcium hydroxide aqueous solution was first injected slowly in the mesoreactor (Figure 1) in order to avoid the formation of bubbles in the system. The orthophosphoric acid aqueous solution was then injected rapidly (3–4 s).

Powder Characterization. Samples were withdrawn at the outlet of the mesoreactor, centrifuged (at 1500 rpm for 5 min), washed twice with ultrapure water and kept in pure ethanol (Koptec 200 proof pure), which stops the solid–liquid reaction.[31] The powders obtained were then characterized by X-ray diffraction (XRD) (PanAlytical X'Pert PRO Alfa-1 diffractometer with $\lambda CuK\alpha = 1.54056$ Å), Fourier transform infrared spectroscopy (FTIR) (Bomem MB-154S), and scanning electron microscopy (SEM) (FEI Quanta 400FEG ESEM/EDAX Genesis X4M with an accelerating voltage of 15 and 20 kV), where samples were covered by a 10 nm layer of gold. For particle size distribution (LS 230, Beckman Coulter), suspensions were collected at the end of each experiment and directly analyzed. As to the Ca/P molar ratio of the final product, total phosphorus was quantified by the ascorbic acid method (spectrophotometer PG Instruments, T60 UV/VIS) and calcium was measured by atomic absorption spectroscopy (spectrometer GBC 932Plus).

Results and Discussion

Mixing study in the meso-OFR operated in batch mode

Hue was measured over time at different locations in the meso-OFR (see Figure 3) and at different mixing conditions. The average values are presented below, being the "Green Hue" the hue value that corresponds to the hue of the solution when the two buffer solutions used are completely mixed.

The results obtained (Figure 4) allow to evaluate the mixing efficiency inside the meso-OFR for the different experimental conditions studied, although in some cases the error bars (corresponding to the standard deviation of each measurement) associated to the hue values are significant, particularly at the bottom of the reactor. Based on Figure 4, it is possible to verify that for $f = 0.83$ Hz and $x_0 = 4.5$ mm, hue values measured at each location rapidly converge to the "Green Hue" value and remain close to this value over time. In relation to the two other cases, it takes longer for the two buffer solutions to mix completely. For $f = 3.67$ Hz and $x_0 = 1$ mm the solutions remain almost unmixed, as hue values at each location except at the bottom of the reactor, practically do not change. Therefore, the best conditions for fast mixing and a more homogeneous reaction medium were assumed to be obtained for $f = 0.83$ Hz and $x_0 = 4.5$ mm.

Precipitation of HAp

Based on the results presented above, precipitation of HAp was carried out in the meso-OFR operated in batch under $f = 0.83$ Hz and $x_0 = 4.5$ mm.

Monitoring of pH. As mentioned before, pH is an important parameter in determining the likelihood of the formation of calcium phosphate phases.[22] Therefore, pH variation over time during HAp precipitation was monitored (Figure 5).

It is important to refer that pH values (see Figure 5) can only be considered for $pH < 8$, as calibration curve *Abs vs. pH* was only linear for pH values between 6.3 and 8. Figure 5 shows that for the mixing Ca/P molar ratios 1.00 and 1.33, pH starts to decrease from approximately 500 s and stabilizes at approximately 2000 and 2500 s, respectively, reaching 6.3 and 6.5, respectively. As to the mixing molar ratio Ca/P = 1.67, pH decreases slowly over time and approaches 7 at approximately 5000 s. Variation of pH over time allows to follow the precipitation reaction, being pH stabilization an indication of the completion of the majority of the reaction. From Figure 5, one can verify that the reaction time increases with Ca/P molar ratio.

According to Table 2, the agreement between final pH values obtained in Figure 5 and final pH values measured by the microelectrode is quite good. Errors bars provide the standard deviation of each measurement.

Phase Identification. Figure 6 shows that single-phased HAp was synthetized for the mixing Ca/P molar ratios 1.33 and 1.67. Diffraction patterns of the prepared powders match well with the diffraction pattern of a reference HAp (JCPDS 9–0432) and a commercial HAp (Spectrum, minimum 40 meshes). However, broader peaks are exhibited, suggesting the presence of amorphous phases or considerably small size particles,[22,23] which is similar to natural bone.[22] Concerning the XRD pattern of the particles that were obtained for the mixing molar ratio Ca/P = 1.00, one can notice the presence of peaks assigned to other calcium phosphates, namely dicalcium phosphate dihydrate (DCPD or brushite) (JCPDS 9–0077). In fact, under weakly acidic aqueous environments

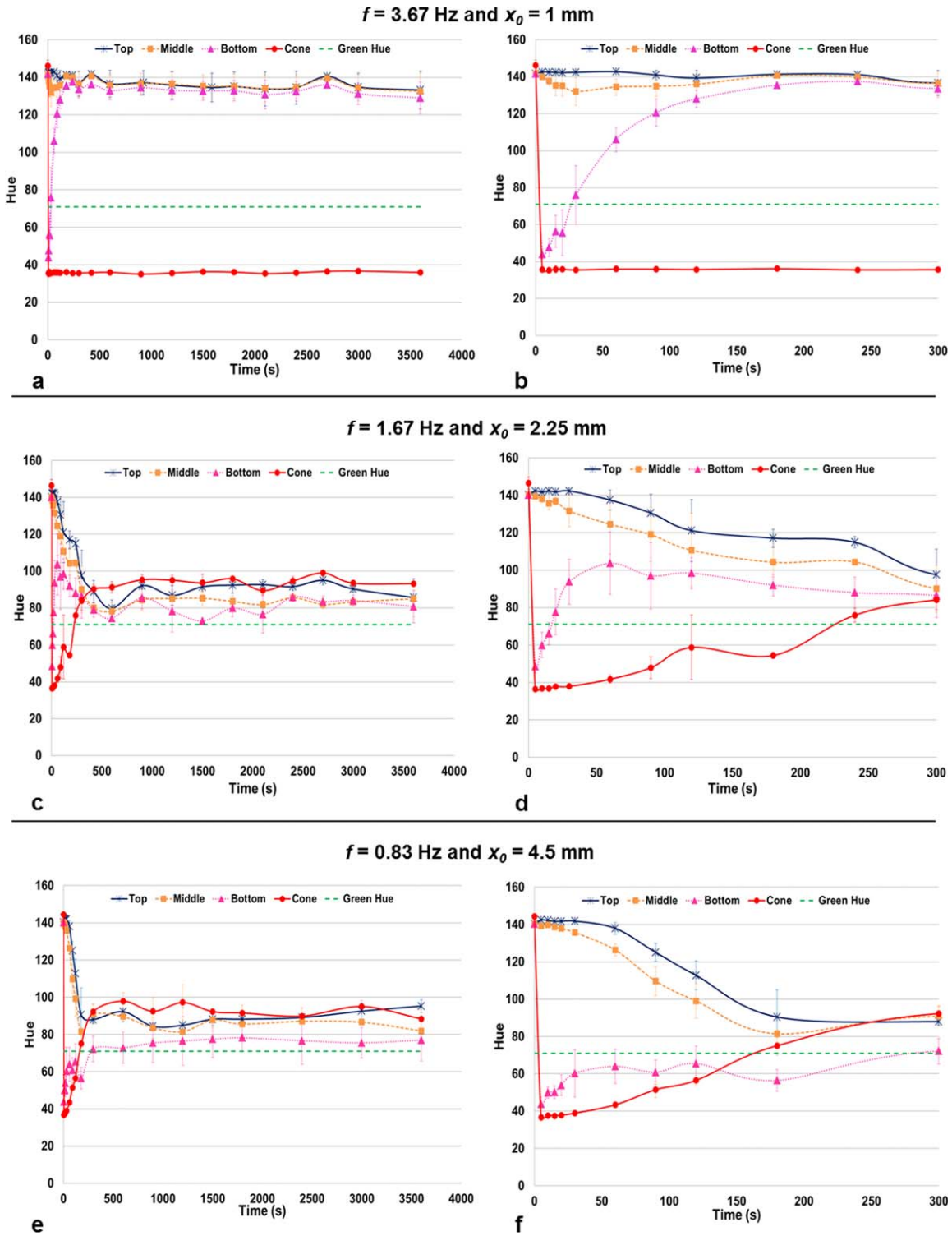

Figure 4. Hue values for different locations in the meso-OFR over time.

[Color figure can be viewed in the online issue, which is available at wileyonlinelibrary.com.]

(pH 4–6), equilibrium conditions can lead to the formation of the brushite phase.[32] Further, brushite grows faster than HAp,[33] the kinetic factors prevailing over the thermodynamics. Sharp and high intensity peaks at 28 °2θ and 40.5 °2θ, assigned to potassium chloride, are observed in the diffraction patterns of the products obtained with the mixing Ca/P molar ratios 1.00 and 1.67. This may be explained by the occlusion of KCl. Indeed, part of the mother liquor could have been trapped between the aggregates, and the KCl contained in the mother liquor crystallized at the drying step.

Based on peaks identified (Figure 7), the synthesis products have a typical apatite structure. Bands of υ_3 PO_4^{3-} mode (around 1037 cm^{-1}) and υ_1 PO_4^{3-} mode (around 962 cm^{-1}) are clearly exhibited in all the spectra, although it is difficult to detect the peak related to υ_4 bending mode of PO_4^{3-}. The broad peak, from approximately 3700 to 3000

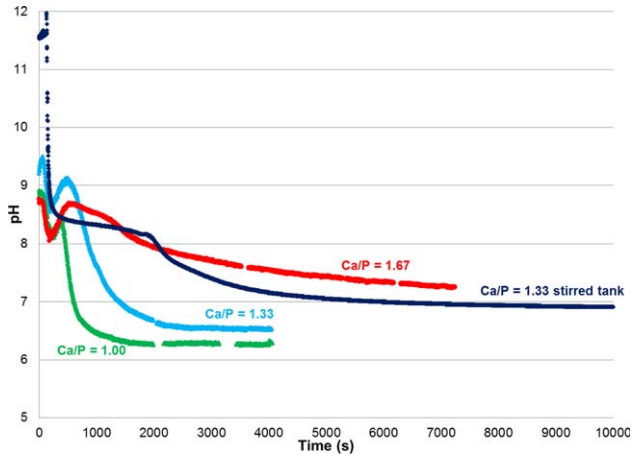

Figure 5. Variation of pH with time during HAp precipitation for different mixing Ca/P molar ratios.

[Color figure can be viewed in the online issue, which is available at wileyonlinelibrary.com.]

cm^{-1}, and the peak at 1643 cm^{-1} (bending mode, υ_2) are assigned to the adsorbed water. This may be justified by the low drying temperature (60°C) and the absence of a ripening (ageing) treatment.[34–36] The peaks assigned to the vibrational mode of OH^- (around 630 cm^{-1}) and to the stretching mode of OH^- (around 3571 cm^{-1}) are also present, although not well resolved. In the case of the peak assigned to the stretching mode of OH^-, this is due to an overlap with the broad band of the adsorbed water (around 3700 to 3000 cm^{-1}).[37] Regarding the vibrational mode of OH^-, the reason why the peak is not clearly visible may be explained by the presence of carbonate ions.[38] Bands at 1454 and 1428 cm^{-1} are indicative of the carbonate ion substitution[35] and are especially observed in the spectrum of the precipitate obtained for the mixing Ca/P molar ratio 1.67, as alkaline solutions readily absorb CO_2.[34] The presence of these bands is characteristic of a carbonated HAp of B-type, where the carbonate ions occupy the phosphate ions sites.[34,36] The small band around 875 cm^{-1} can be attributed to the vibrational frequencies of carbonate ions or HPO_4^{2-} group,[35] which is consistent with a carbonated HAp or calcium-deficient HAp. The noise observed in the commercial HAp spectrum (1800 to 1400 cm^{-1}) is due to water vapor.

Precipitates were also characterized in terms of their final Ca/P molar ratio (see Table 2). According to Table 2, precipitates are nonstoichiometric HAp, as their molar ratio is different from the stoichiometric value. The product obtained for the mixing Ca/P molar ratio 1.67 seems to be calcium deficient HAp, once its Ca/P molar ratio is lower than 1.67. Actually, HAp is a compound with a variable composition existing over Ca/P molar ratios from 1.67 for stoichiometric to ~1.5 for fully calcium deficient HAp,[22] and sometimes even outside this range.[39] Regarding the Ca/P molar ratio of the final product obtained for the mixing Ca/P molar ratio 1.33, it is higher than the stoichiometric value showing, therefore, the formation of a carbonated HAp of B-type.[1,38]

Particle Size, Size Distribution, and Morphology. According to Figure 8, particle size distributions for all the mixing molar ratios studied are similar. The as-prepared particles mainly consist in particles at the nanometer range with a mean size of about 67 nm. Particles are, therefore, of the same order of magnitude of the commercial HAp particles (Spectrum, minimum 40 meshes), originally submitted to granulometric separation. It is very important to underline that particles produced were directly obtained from the experimental system without thermal treatment and without granulometric separation. Besides, the results reveal that this distribution is narrower for particles formed in the meso-OFR than for the commercial powder.

SEM images (Figure 9) corresponding to particles obtained for the mixing molar ratio Ca/P = 1.00 show two types of crystals: crystals that exhibit well defined platelet morphology and a smooth surface, with an average crystallite size around 10–20 μm, and aggregated plate-shaped crystals with crystallites at the nanometer range. The well-defined platelet morphology is characteristic of DCPD[37,40] and the nanocrystallites are characteristic of HAp.[41] As mentioned before, DCPD could also be precipitated in the present operating

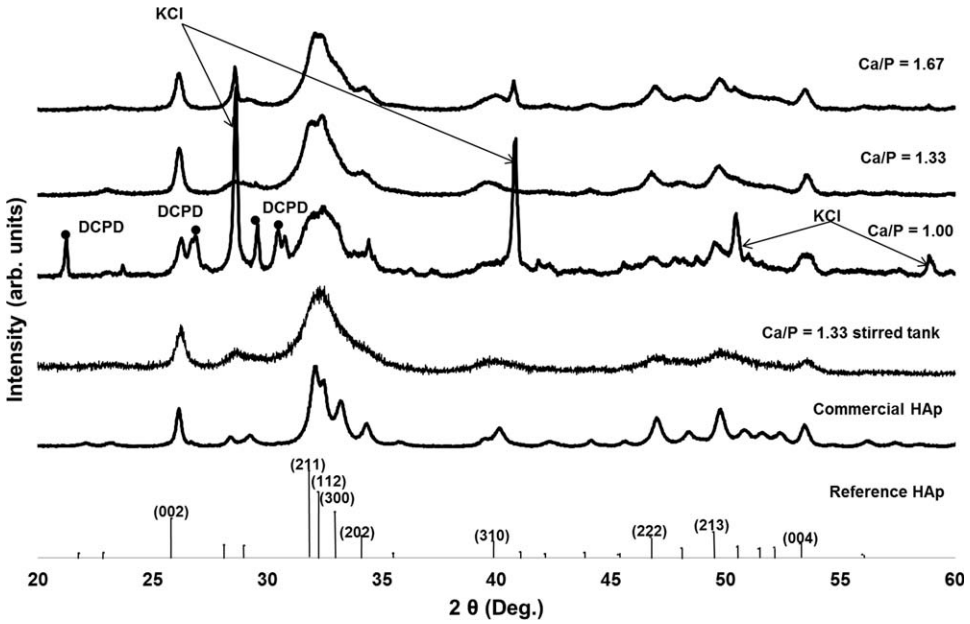

Figure 6. XRD patterns of the particles produced for different mixing Ca/P molar ratios.

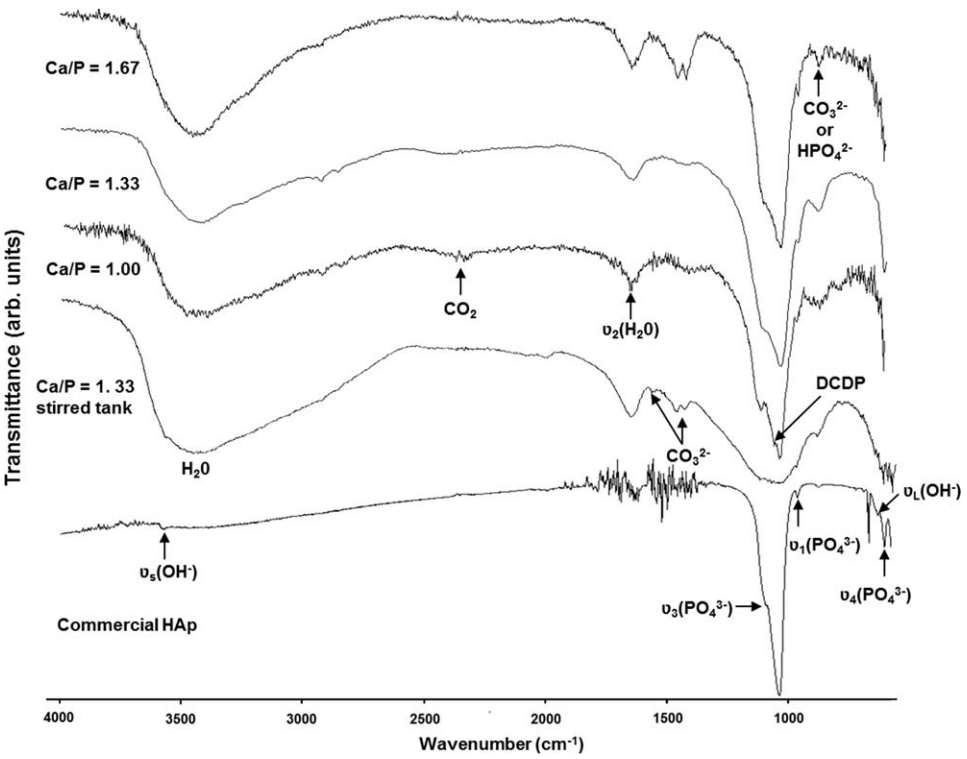

Figure 7. FTIR spectra of the particles produced for different mixing Ca/P molar ratios.

conditions. DCPD, which easily forms a plate-shaped crystal morphology,[41] could then be transformed into HAp by maintaining the plate-shaped particle morphology. Concerning the mixing Ca/P molar ratios 1.33 and 1.67, powders mostly consist of crystals exhibiting a plate-like (predominant) and rod-like morphology with typical sizes in the nanometer range, being in agreement with the literature. According to Neira et al.,[42] phase-pure HAp products can be characterized as either rod-like (whiskers, needles, wires, fibers, etc.) or plate-like. Further, the precipitated particles for the mixing molar ratio Ca/P = 1.67 seem slightly bigger and have a well-defined morphology when compared to the precipitated particles for the mixing molar ratio Ca/P = 1.33.

Based on the results presented above, the mixing molar ratio Ca/P = 1.33 was chosen for the continuation of the work, once stable HAp nanoparticles were generated faster and under near-physiological conditions of temperature and pH. This is particularly important when preparing HAp for medical purposes. Indeed, it is important to follow specific criteria for pH and temperature in order to promote more conductive conditions for the survival of bone-related cells.[1]

Comparative study of HAp precipitation for the meso-OFR operated in batch and a stirred tank batch reactor

HAp nanoparticles prepared under the optimized experimental conditions in a stirred tank batch reactor[27] and in the meso-OFR operated in batch were compared. HAp precipitation process was carried out in both reactors under the same conditions of temperature (37 °C), mixing Ca/P molar ratio (Ca/P = 1.33), and power density (31.5 $W \cdot m^{-3}$). The constant power density applied to both reactors was used as the reference criterion in this comparative study. Despite mixing mechanisms being different in each system, and thereby hydrodynamic conditions being not directly comparable, this criterion is quite informa-

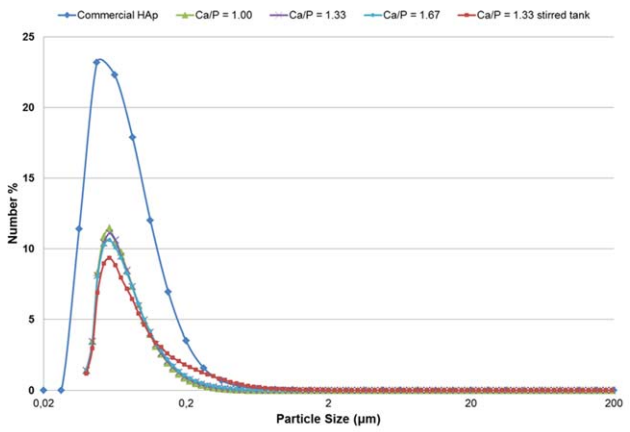

Reactor	Mixing Ca/P molar ratio	Particles size (µm)			Span
		d_{10}	d_{50}	d_{90}	
Meso-OFR operated in batch	1.00	0.046	0.066	0.125	1.18
	1.33	0.047	0.067	0.123	1.23
	1.67	0.047	0.068	0.134	1.29
Stirred tank batch reactor	1.33	0.047	0.074	0.209	2.18
Commercial HAp	-	0.034	0.058	0.130	1.64

Figure 8. Particle size distribution in number and parameters of the particle size distribution in number of the particles produced for different mixing Ca/P molar ratios.

d_{10}: 10% of the particles are smaller than this value, d_{50}: 50% of the particles are smaller than this value; d_{90}: 90% of the particles are smaller than this value; span: width of the distribution based on the 10, 50, and 90% quantile. [Color figure can be viewed in the online issue, which is available at wileyonlinelibrary.com.]

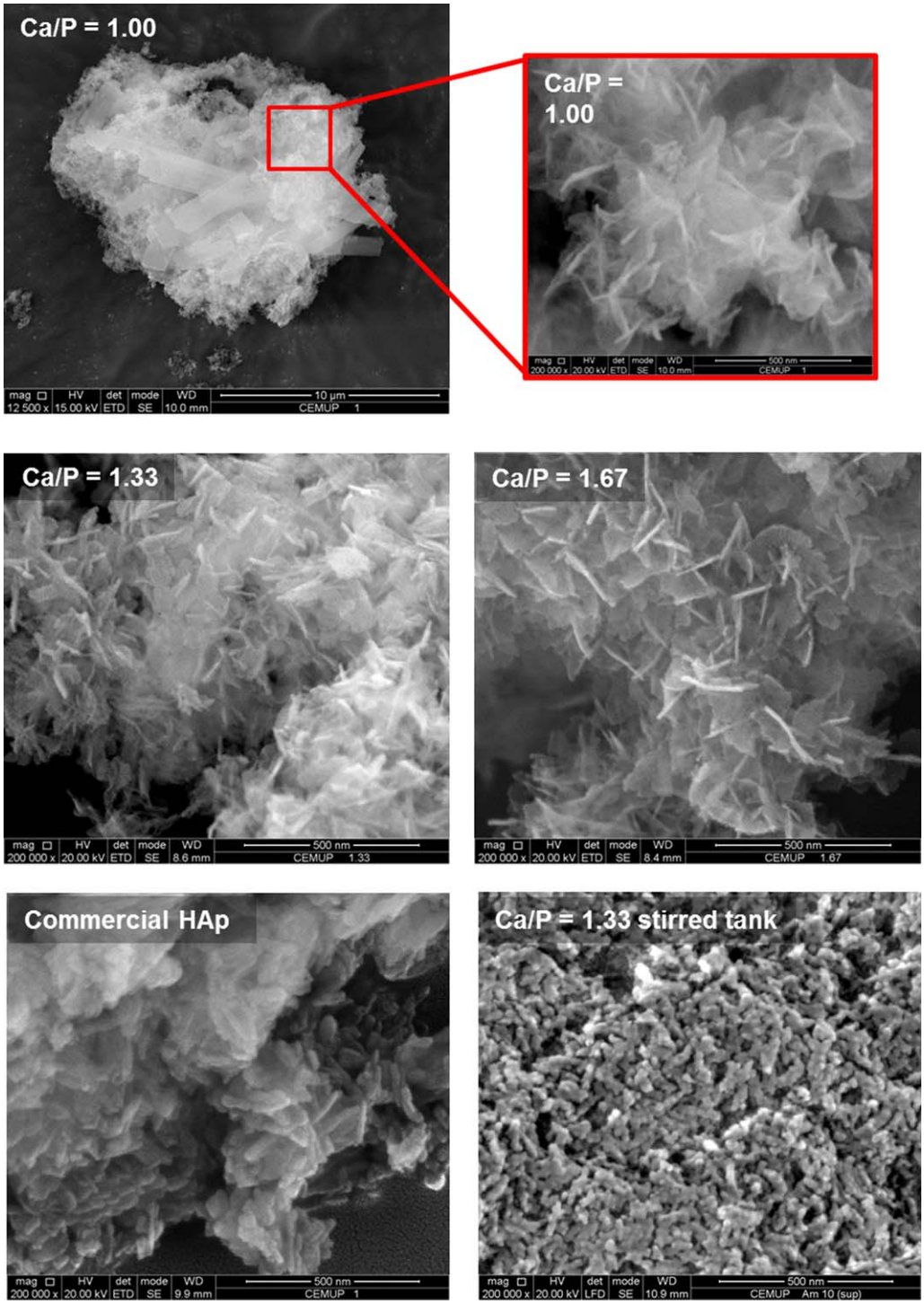

Figure 9. SEM images of the particles obtained for different mixing Ca/P molar ratios.

[Color figure can be viewed in the online issue, which is available at wileyonlinelibrary.com.]

tive, because it enables assessing the effectiveness of both reactors for a given power input, in terms of reaction time and quality of the precipitated particles.

According to Figure 5, pH stabilizes at approximately 2500 s in the meso-OFR, whereas in the stirred tank batch reactor pH stabilizes around 10000 s, meaning that the majority of the precipitation reaction is completed about four times faster in the meso-OFR.

The diffraction patterns (see Figure 6) indicate that the HAp prepared in the stirred tank batch reactor is single-phased HAp with low crystallinity degree compared with the diffraction pattern of the HAp prepared in the meso-OFR operated in batch. This result is also confirmed by the FTIR spectra. Based on Figure 7, HAp prepared in the stirred tank is more amorphous, as its spectrum exhibits broader peaks, especially phosphate characteristic bands at 900–1200 cm^{-1}. Besides, carbonate contamination seems to be minimized in the meso-OFR, as carbonate bands at approximately 1454 and 1428 cm^{-1} are barely detected in the spectrum of the powder obtained in the meso-OFR (see Figure 7).

Based on particle size distributions (Figure 8), as-prepared HAp particles are mainly composed by primary particles at the nanometer range, in both the meso-OFR and the stirred tank. Further, it is possible to confirm that HAp particles prepared in the meso-OFR have a smaller primary particle size and a narrower size distribution when compared with the size distribution of HAp particles prepared in the stirred tank.

Figure 9 reveals the characteristic morphology of precipitated HAp particles produced in each reactor. It can be observed that HAp nanoparticles prepared in the stirred tank reactor show typical rod-like shape, whereas HAp nanoparticles prepared in the meso-OFR mostly consist in plate-shaped HAp particles, although some particles appear to be rod-like shaped.

In short, this work showed the feasibility of using a meso-OFR for process intensification for HAp nanoparticles production. By comparison with a stirred tank reactor, the proposed meso-OFR has the capacity of yielding HAp nanoparticles about four times faster. Further, the mesoreactor yielded HAp particles with improved characteristics, namely higher crystallinity, smaller size, and narrower size distribution. Moreover, the meso-OFR is a mesoscale (milliliter) device, thus reducing reagent requirements and waste generated.

Conclusions

Precipitation of HAp was investigated in a vertical meso-OFR operated batchwise under near physiological conditions of pH and temperature. Mixing efficiency of the meso-OFR under batch operation was first evaluated. Values of $f = 0.83$ Hz and $x_0 = 4.5$ mm were proved to be the best operating conditions for fast mixing and more homogeneous reaction environment, that is, conditions that favor the formation of small and uniform HAp particles with consistent characteristics. Precipitation of HAp was then carried out for different mixing Ca/P molar ratios, formation of single-phased calcium-deficient and/or B-type carbonated HAp being confirmed for the mixing Ca/P molar ratios 1.33 and 1.67. It also has been shown that for the mixing molar ratio Ca/P = 1.33, stable HAp nanoparticles were obtained at a pH close to 7, which is particularly important in the preparation of HAp for medical purposes.

Constant power density was used as the reference operation criterion applied to the meso-OFR operated in batch and to a stirred tank batch reactor. This enabled comparing the performance of both reactors, in terms of reaction time and quality of the precipitated particles, for a given power input. Based on the aforementioned results, it was concluded that the reactor type affects crystallinity, carbonate content, morphology, size, and size distribution of the as-prepared HAp nanoparticles. In the proposed meso-OFR, operated under oscillatory flow, HAp nanoparticles were generated about four times faster than in the stirred tank batch reactor operated under a similar power density. Further, HAp particles showed improved characteristics, namely higher crystallinity, smaller size, and narrower size distribution. Therefore, the meso-OFR proved to be more efficient in the production of HAp nanoparticles while also rendering the process cleaner and safer due to the reduction of waste generated and reagents requirements, making it an interesting tool for high throughput experimentation.

Finally, we believe that even if the reactor studied in this work does not represent a full scale production unit, it may be a useful contribution to the development of a platform for the production of valuable and high-quality HAp nanoparticles.

Acknowledgments

This work was supported by the Portuguese Foundation for Science and Technology (SFRH/BD/42992/2008) through the MIT-Portugal Program, Bioengineering Systems Focus *Area*. The authors are thankful to Dr Jorge Ferreira from LNEG (Laboratório Nacional de Energia e Geologia, Portugal) for carrying out the X-ray measurements and his help with the interpretation of results.

Notation

C_D = baffle discharge coefficient
d_{10} = 10% of the particles are smaller than this value
d_{50} = 50% of the particles are smaller than this value
d_{90} = 90% of the particles are smaller than this value
D = diameter of the tube, m
D_0 = diameter of the constriction, m
D_s = diameter of the stirrer, m
D_t = diameter of the tank, m
f = oscillation frequency, Hz
L = height of the tank, m
N = speed of the stirrer, s^{-1}
N_B = number of constrictions per unit length, m^{-1}
N_P = power number of the stirrer
P/V = power density, W m^{-3}
Re = Reynolds number
span = width of the distribution based on the 10, 50, and 90% quantile
x_0 = oscillation amplitude, m (center-to-peak)

Greek letters

α = baffle free area ratio
ρ = fluid density, kg m^{-3}
ω = oscillation angular frequency, rad s^{-1}

Literature Cited

1. Kumta PN, Sfeir C, Lee D-H, Olton D, Choi D. Nanostructured calcium phosphates for biomedical applications: novel synthesis and characterization. *Acta Biomater*. 2005;1:65–83.
2. Gomez-Morales J, Torrent-Burgues J, Rodriguez-Clemente R. Crystal size distribution of hydroxyapatite precipitated in a MSMPR reactor. *Cryst Res Technol*. 2001;36:1065–1074.
3. Wang F, Li M-S, Lu Y-P, Qi Y-X, Liu Y-X. Synthesis and microstructure of hydroxyapatite nanofibers synthesized at 37°C. *Mater Chem Phys*. 2006;95:145–149.
4. Kuznetsov A, Fomin A, Veresov A, Putlyaev V, Fadeeva I, Barinov S. Hydroxyapatite of platelet morphology synthesized by ultrasonic precipitation from solution. *Russ J Inorg Chem*. 2008;53:1–5.
5. Jones A, Rigopoulos S, Zauner R. Crystallization and precipitation engineering. *Comput Chem Eng*. 2005;29:1159–1166.
6. Chew CM, Ristic RI. Crystallization by oscillatory and conventional mixing at constant power density. *AIChE J*. 2005;51:1576–1579.
7. Ristic R. Oscillatory mixing for crystallization of high crystal perfection pharmaceuticals. *Chem Eng Res Des*. 2007;85:937–944.
8. Fitch AW, Jian H, Ni X. An investigation of the effect of viscosity on mixing in an oscillatory baffled column using digital particle image velocimetry and computational fluid dynamics simulation. *Chem Eng J*. 2005;112:197–210.
9. Mackley MR, Smith KB, Wise NP. The mixing and separation of particle suspensions using oscillatory flow in baffled tubes. *Chem Eng Res Des*. 1993;71:649–656.
10. Reis N. Novel Oscillatory Flow Reactors for Biotechnological Applications. 2006, PhD thesis. Braga, Portugal.
11. Ni X, Jian H, Fitch AW. Computational fluid dynamic modeling of flow patterns in an oscillatory baffled column. *Chem Eng Sci*. 2002; 57:2849–2862.
12. Ni X, Sommer Y, Gélicourt D, Neil J, Howes T. On the effect of tracer density on axial dispersion in a batch oscillatory baffled column. *Chem Eng J*. 2002;85:17–25.

13. Reis N, Harvey A, Mackley MR, Vicente AA, Teixeira JA. Fluid mechanics and design aspects of a novel oscillatory flow screening mesoreactor. *Chem Eng Res Des*. 2005;83:357–371.
14. Reis N, Vicente AA, Teixeira JA, Mackley MR. Residence times and mixing of a novel continuous oscillatory flow screening reactor. *Chem Eng Sci*. 2004;59:4967–4974.
15. Lopes AM, Silva DP, Vicente AA, Pessoa A Jr, Teixeira JA. Aqueous two-phase micellar systems in an oscillatory flow micro-reactor: study of perspectives and experimental performance. *J Chem Technol Biotechnol*. 2011;86:1159–1165.
16. Simon LL, Abbou Oucherif K, Nagy ZK, Hungerbuhler K. Bulk video imaging based multivariate image analysis, process control chart and acoustic signal assisted nucleation detection. *Chem Eng Sci*. 2010;65:4983–4995.
17. Brown CJ, Ni X. Online evaluation of paracetamol antisolvent crystallization growth rate with video imaging in an oscillatory baffled crystallizer. *Cryst Growth Des*. 2011;11:719–725.
18. Brown CJ, Ni XW. Evaluation of growth kinetics of antisolvent crystallization of paracetamol in an oscillatory baffled crystallizer utilizing video imaging. *Cryst Growth Des*. 2011;11:3994–4000.
19. Brown CJ, Ni XW. Determination of metastable zone width, mean particle size and detectable number density using video imaging in an oscillatory baffled crystallizer. *CrystEngComm*. 2012;14:2944–2949.
20. Simon LL, Myerson AS. Continuous antisolvent plug-flow crystallization of a fast growing API. *18th International Symposium on Industrial Crystallization - ISIC 18*. Zurich, Switzerland, 2011.
21. Shekunov BY, York P. Crystallization processes in pharmaceutical technology and drug delivery design. *J Cryst Growth*. 2000;211:122–136.
22. Wang L, Nancollas GH. Calcium orthophosphates: crystallization and dissolution. *Chem Rev*. 2008;108:4628–4669.
23. Lynn AK, Bonfield W. A novel method for the simultaneous, titrant-free control of pH and calcium phosphate mass yield. *Acc Chem Res*. 2005;38:202–207.
24. Cabaret F, Bonnot S, Fradette L, Tanguy PA. Mixing time analysis using colorimetric methods and image processing. *Ind Eng Chem Res*. 2007;46:5032–5042.
25. Rezk AR, Qi A, Friend JR, Li WH, Yeo LY. Uniform mixing in paper-based microfluidic systems using surface acoustic waves. *Lab Chip*. 2012;12:773–779.
26. Florea L, Fay C, Lahiff E, Phelan T, O'Connor NE, Corcoran B, Diamond D, Benito-Lopez F. Dynamic pH mapping in microfluidic devices by integrating adaptive coatings based on polyaniline with colorimetric imaging techniques. *Lab Chip*. 2013;13:1079–1085.
27. Castro F, Ferreira A, Rocha F, Vicente A, Teixeira JA. Characterization of intermediate stages in the precipitation of hydroxyapatite at 37 °C. *Chem Eng Sci*. 2012;77:150–156.
28. Ni X, Gao S, Cumming RH, Pritchard DW. A comparative study of mass transfer in yeast for a batch pulsed baffled bioreactor and a stirred tank fermenter. *Chem Eng Sci*. 1995;50:2127–2136.
29. Haynes WM. CRC Handbook of Chemistry and Physics, 93rd ed. Taylor & Francis, Boca Raton, 2012.
30. Johannsen K, Rademacher S. Modelling the kinetics of calcium hydroxide dissolution in water. *Acta Hydroch Hydrob*. 1999;27:72–78.
31. Bernard L, Freche M, Lacout J, Biscans B. Modeling of the dissolution of calcium hydroxide in the preparation of hydroxyapatite by neutralization. *Chem Eng Sci*. 2000;55:5683–5692.
32. Lee D, Kumta PN. Chemical synthesis and stabilization of magnesium substituted brushite. *Mater Sci Eng C*. 2010;30:934–943.
33. Ferreira A, Oliveira C, Rocha F. The different phases in the precipitation of dicalcium phosphate dihydrate. *J Cryst Growth*. 2003;252:599–611.
34. Osaka A, Miura Y, Takeuchi K, Asada M, Takahashi K. Calcium apatite prepared from calcium hydroxide and orthophosphoric acid. *J Mater Sci Mater Med*. 1991;2:51–55.
35. Koutsopoulos S. Synthesis and characterization of hydroxyapatite crystals: a review study on the analytical methods. *J Biomed Mater Res*. 2002;62:600–612.
36. Zhou W, Wang M, Cheung W, Guo B, Jia D. Synthesis of carbonated hydroxyapatite nanospheres through nanoemulsion. *J Mater Sci Mater Med*. 2008;10:103–110.
37. Panda RN, Hsieh MF, Chung RJ, Chin TS. FTIR, XRD, SEM and solid state NMR investigations of carbonate-containing hydroxyapatite nano-particles synthesized by hydroxide-gel technique. *J Phys Chem Solids*. 2003;64:193–199.
38. Nelson DG, Featherstone JD. Preparation, analysis, and characterization of carbonated apatites. *Calcif Tissue Int*. 1982;34:S69–S81.
39. Elliot JC. Structure and Chemistry of the Apatites and Other Calcium Orthophosphates. Amsterdam: Elsevier, 1994.
40. Siddharthan A, Seshadri SK, Kumar TSS. Rapid synthesis of calcium deficient hydroxyapatite nanoparticles by microwave irradiation. *Trends Biomater Artif Organs*. 2005;18:110–113.
41. Zhuang Z, Yamamoto H, Aizawa M. Synthesis of plate-shaped hydroxyapatite via an enzyme reaction of urea with urease and its characterization. *Powder Technol*. 2012;222:193–200.
42. Neira IS, Kolen'ko YV, Lebedev OI, Tendeloo GV, Gupta HS, Guitian F, Yoshimura M. An effective morphology control of hydroxyapatite Crystals via Hydrothermal synthesis. *Cryst Growth Des*. 2009;9:466–474.

Manuscript received Mar. 5, 2013, and revision received July 2, 2013.